Impact of suborbital climate changes in the North Atlantic on ice sheet dynamics at the Mid-Pleistocene Transition

I. Hernández-Almeida,[1,2] F. J. Sierro,[1] I. Cacho,[3] and J. A. Flores[1]

Received 3 August 2011; revised 18 June 2012; accepted 20 June 2012; published 16 August 2012.

[1] Early and Mid-Pleistocene climate, ocean hydrography and ice sheet dynamics have been reconstructed using a high-resolution data set (planktonic and benthic $\delta^{18}O$ time series, faunal-based sea surface temperature (SST) reconstructions and ice-rafted debris (IRD)) record from a high-deposition-rate sedimentary succession recovered at the Gardar Drift formation in the subpolar North Atlantic (Integrated Ocean Drilling Program Leg 306, Site U1314). Our sedimentary record spans from late in Marine Isotope Stage (MIS) 31 to MIS 19 (1069–779 ka). Different trends of the benthic and planktonic oxygen isotopes, SST and IRD records before and after MIS 25 (~940 ka) evidence the large increase in Northern Hemisphere ice-volume, linked to the cyclicity change from the 41-kyr to the 100-kyr that occurred during the Mid-Pleistocene Transition (MPT). Beside longer glacial-interglacial (G-IG) variability, millennial-scale fluctuations were a pervasive feature across our study. Negative excursions in the benthic $\delta^{18}O$ time series observed at the times of IRD events may be related to glacio-eustatic changes due to ice sheets retreats and/or to changes in deep hydrography. Time series analysis on surface water proxies (IRD, SST and planktonic $\delta^{18}O$) of the interval between MIS 31 to MIS 26 shows that the timing of these millennial-scale climate changes are related to half-precessional (10 kyr) components of the insolation forcing, which are interpreted as cross-equatorial heat transport toward high latitudes during both equinox insolation maxima at the equator.

Citation: Hernández-Almeida, I., F. J. Sierro, I. Cacho, and J. A. Flores (2012), Impact of suborbital climate changes in the North Atlantic on ice sheet dynamics at the Mid-Pleistocene Transition, *Paleoceanography*, *27*, PA3214, doi:10.1029/2011PA002209.

1. Introduction

[2] The so-called "Mid-Pleistocene Transition" (MPT) is defined as the period in which the climatic cyclicity shifted from the ~41-kyr cycles, related to obliquity, to the ~100-kyr cycles, related to eccentricity [*Berger and Jansen*, 1994]. During the "41-kyr world," continental ice sheets were reduced in size and glacial periods milder compared to those during the "100-kyr world" [*Clark et al.*, 2006], which led to dramatic reorganizations in the global climatic system. Records from Northern Hemisphere and time series modeling document the glacial expansion during this period [*Barendregt and Irving*, 1998; *Heslop et al.*, 2002; *Maslin and Ridgwell*, 2005; *Mudelsee and Stattegger*, 1997; *Muttoni et al.*, 2003; *Prell*, 1982] and its impact on global climate and ocean circulation [*Ferretti et al.*, 2005; *McClymont et al.*, 2008; *Raymo et al.*, 1997, 2004; *Schmieder et al.*, 2000]. A precise knowledge of this period of global reorganization is essential for the better understanding of the Pleistocene climate evolution in a broader context.

[3] One of the most intriguing questions is whether orbital and suborbital climate variability was exclusive of Late Pleistocene records [e.g., *Bond et al.*, 1992, 1997; *Cortijo et al.*, 2000; *Elliot et al.*, 1998; *Oppo et al.*, 1998; *Shackleton et al.*, 2000; *Siddall et al.*, 2006], or were also present in older sedimentary sequences. For this purpose, scientific ocean drilling community has concentrated its attention on sediment drifts, which provide ideal long cores with high-sedimentation rates for paleoclimatic and paleoceanographic research. After the pioneering studies of *McManus et al.* [1999] that related the millennial-scale climate oscillations observed at Site 980 during the last 500 kyr with instabilities associated to excess ice, various studies have addressed millennial climate variability over the last million years. A 124-kyr record of benthic and planktonic stable isotopes led *Ferretti et al.* [2010] to conclude that high-frequency climate oscillations at Site U1313 correspond to harmonics of the precession cycles. High-resolution studies at Site 983

[1]Department of Geology, University of Salamanca, Salamanca, Spain.
[2]Now at Institute of Geography and Oeschger Centre for Climate Change Research, University of Bern, Bern, Switzerland.
[3]GRC Marine Geosciences, Department of Stratigraphy, Paleontology and Marine Geosciences, University of Barcelona, Barcelona, Spain.

Corresponding author: I. Hernández-Almeida, Institute of Geography and Oeschger Centre for Climate Change Research, University of Bern, Erlachstr. 9a, CH-3012 Bern, Switzerland. (ivan.hernandez@giub.unibe.ch)

0883-8305/12/2011PA002209

reported by *Kleiven et al.* [2003, 2011] established that millennial-scale events of poor ventilation during ice sheet decay events and the release of meltwater to the North Atlantic were a persistent feature during the Mid-Pleistocene. *Hodell et al.* [2008] found frequent millennial-scale IRD fluctuations reflected by Si/Sr peaks at Site U1308, related to climate-driven changes in the mass balance of ice sheets. In addition, several authors have observed similar millennial-scale climate instability in the North Atlantic during the Pliocene epoch [e.g., *Bartoli et al.*, 2006; *Bolton et al.*, 2010; *Hayashi et al.*, 2010; *McIntyre et al.*, 2001; *Niemitz and Billups*, 2005; *Ortiz et al.*, 1999].

[4] All these observations suggest that some boundary conditions associated with millennial-climate scale variability were already surpassed before the establishment of the 100-kyr cycles from the Late Pleistocene. The mechanism triggering these millennial-scale instabilities is still controversial, but several studies point toward a low-latitude insolation origin, through ocean-atmosphere-ice sheet coupling, that would explain the presence of these fluctuations before the establishment of high-amplitude 100-kyr glacial cycles [*Hagelberg et al.*, 1994; *McIntyre and Molfino*, 1996; *Short et al.*, 1991; *Weirauch et al.*, 2008].

[5] Most of these studies, however, were mainly based on stable isotope or ice-rafted debris (IRD) records. In order to offer new insights we performed an integrated study based on high resolution records of different proxies such as ice-rafted debris (IRD), faunal-based sea surface temperatures (SST) reconstructions and δ^{18}O benthic and planktonic records that revealed the occurrence of precession harmonics in the North Atlantic before the MPT. The combination of SST and planktonic δ^{18}O records that were used as proxies for sea surface circulation in the North Atlantic, changes of IRD mainly linked to ice sheet instabilities and the benthic δ^{18}O variations associated to deep-water circulation allowed us to reconstruct a unique record of the interaction between ice sheet dynamics and climate change in the North Atlantic for the time period between 1069 and 779 ka. Location of Site U1314, close to the IRD belt and within the main core of the North Atlantic Deep Water (NADW), makes it sensitive to changes in the mass balance of continental ice sheets from North Atlantic, and the high sedimentation rates of the Gardar Drift allows to establish a detailed record of climate and ocean variability at orbital and suborbital timescales. Here we investigate the behavior of the climate system in the subpolar North Atlantic in relation with insolation changes in the Equator, through coupling of the ocean, the atmosphere, and ice sheets on the suborbital scale.

2. Regional Settings

[6] IODP Site U1314 (2820 m) was cored by the D/V JOIDES Resolution in the southern Gardar Drift, in the subpolar North Atlantic (56.36°N, 27.88°W) during IODP Expedition 306 (Figure 1). This site is located inside the subpolar gyre, in the path of an extension of the North Atlantic Current (NAC). Today, as during interglacial periods, the warm NAC carries heat and moisture toward the pole. Between 53°N and 60°N, Irminger current (IC) splits from the NAC and turns toward the Greenland coast mixing with the cold East Greenland Current (EGC), which then mixes with the Labrador Current (LC) westward. The main NAC flows into Greenland-Iceland-Norwegian (GIN) Seas, where is cooled, increasing its density [*Krauss*, 1986; *Schmitz and McCartney*, 1993]. Winter convection of the cooled Atlantic surface waters results in the formation of North Atlantic Deep Water (NADW), which flows southward as the Iceland-Scotland Overflow Water (ISOW) (Figure 1). This water mass bathes Site U1314 and control sedimentation over the Gardar Drift [*Bianchi and McCave*, 2000].

[7] Site U1314 is seasonally affected by the southward extension of the Arctic Front (AF), which marks the maximum extent of winter sea-ice [*Swift and Aagaard*, 1981] and is the boundary between the cold arctic waters of the EGC and the warm Atlantic waters of the NAC. Lying south of the AF, seasonal SSTs mean value of _12°C and salinity of 35 ‰, while at northern latitudes, within the arctic domain, temperatures are <−1°C, 30–33‰ [*Conkright et al.*, 1998]. Although today AF lies north of Site U1314, it is known to have migrated southward during glacials of the Pleistocene bringing much cooler waters and potentially also sea-ice south of 60°N [*Ruddiman*, 1977; *Wright and Flower*, 2002].

3. Material and Methods

[8] Early and Mid-Pleistocene sediments at Site U1314 consist predominantly of biogenic oozes with varying proportion of calcareous (e.g., nannofossils and foraminifers) and siliceous organisms (e.g., diatoms and radiolarians) and lower content of terrigenous components, such as quartz, volcanic material and clay. More detailed core description is given in Site U1314 summary [*Channell et al.*, 2006].

[9] Samples from Site U1314 were taken every 4 cm between the 60 to 84.16 m composite depth (mcd). Each sample was wet sieved with distilled water over a 63 μm mesh and both coarse and fine fractions recovered, dried at 40°C and weighed. Later, the sample was dry sieved into two fractions, 63–150 μm and >150 μm. The relative abundance of planktonic foraminifer and the coarse-grained ice-rafted debris per gram (IRD/g) were determined by examination of the >150 μm size fraction.

[10] Full census counts were completed for every other sample. Each sample was split to about 400 planktonic foraminifers, then species of planktonic and benthic foraminifers, as well as mineral grains, ash, lithic fragments, radiolarians, ostracodes and planktonic foraminifer fragments were counted under a binocular microscope, and relative percentages and particle/individuals per gram were calculated. The planktonic foraminifer fauna is characterized by polar, subpolar and transitional species. The dominant species are *Neogloboquadrina pachyderma* sinistrorsa (sin.), *Neogloboquadrina pachyderma* dextrorsa (dex.), *Globigerina bulloides*, *Globorotalia inflata* and *Turborotalita quinqueloba.* Based on these counts we performed a sea surface temperature estimation by running a transfer function based on a back propagation artificial neural network (ANN) [*Malmgren et al.*, 2001] trained on the North Atlantic MARGO Project data set [*Kucera et al.*, 2005]. Additionally, we applied a Modern Analog Technique (MAT) [*Prell*, 1985] to the faunal counts with the same modern data set. For the ANN, a set of ten neural networks was considered, and thus ten different mean annual temperatures were obtained. The average of these 10 temperatures is the final

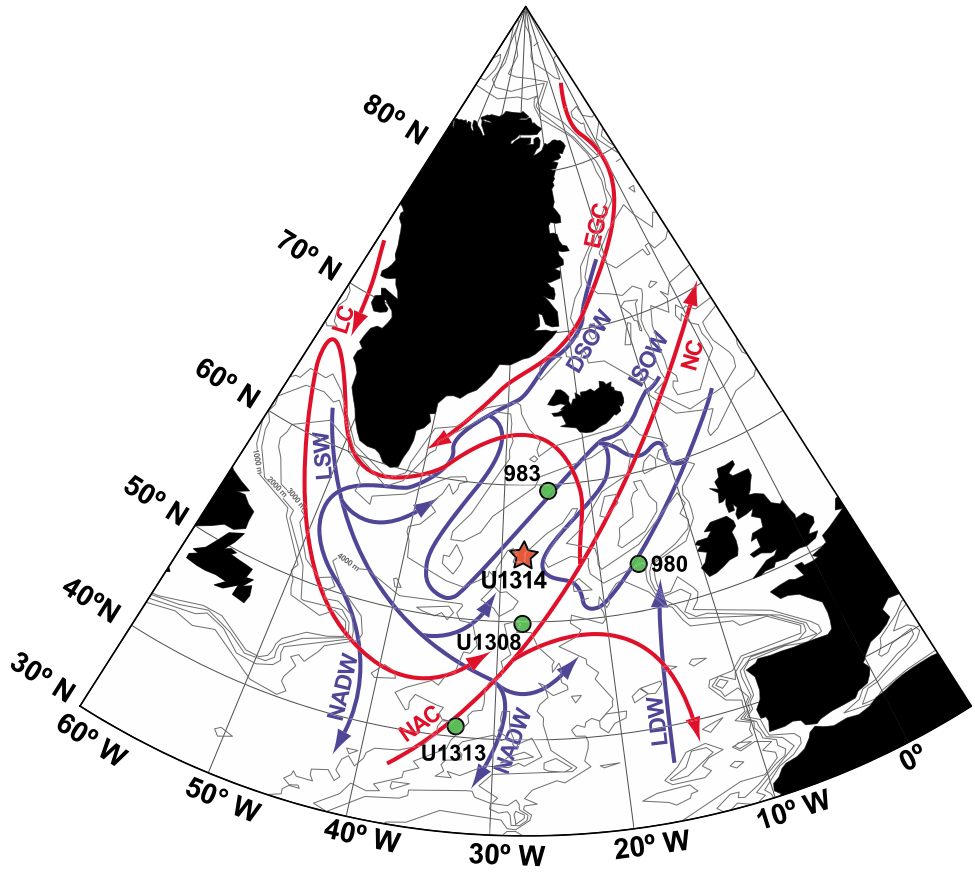

Figure 1. Location of IODP Site U1314 (red star: 56°21′N, 27°W; 2820 m water depth), and other North Atlantic sites (see Table 2). Modern surface (red), and deep circulation (blue) in the North Atlantic [*Krauss*, 1986; *Schmitz and McCartney*, 1993]. Map generated with Ocean Data View v.3.4.3. software (R. Schlitzer, 2008, available at http://odv.awi.de). East Greenland Current (EGC), Norwegian Current (NC), Labrador Current (LC), North Atlantic Current (NAC), Irminger Current (IC), Denmark Strait Overflow Water (DSOW), Iceland Scotland Overflow Water (ISOW), Labrador Sea Water (LSW), North Atlantic Deep Water (NADW), and Lower Deep Water (LDW).

value used for the reconstruction. Standard deviation (StDev) of the ten networks reflects how well the sample is represented in the calibration data set. For the MAT, we applied a set of ten modern analogues and calculated a similarity index.

[11] Benthic stable isotope analyses were carried on *Cibicidoides* spp. (mainly *C. wuellerstorfi* and occasionally *C. pachyderma*), an epifaunal benthic foraminifer species. One to eight tests of *Cibicidoides* were picked from the >250 μm size fraction and one to eight individuals were used for isotopic analysis. When this species was absent, we picked specimens of *Melonis pompilioides* from the same size fraction to produce a continuous signal. *M. pompilioides* is a mid-depth infaunal species [*Corliss*, 1985, 1991; *Duplessy et al.*, 1984; *McCorkle et al.*, 1990] and stable isotope results based on this species should be carefully interpreted. In order to construct a continuous isotope record from both species, we calculated the mean difference between both species in 74 samples covering the 1069 to 400 ka period [*Alonso-Garcia et al.*, 2011; this study]. The StDev between offsets was 0.52 for the carbon and 0.12 for the oxygen. The average difference is −0.11‰ for the oxygen and +0.6‰ for the carbon isotopes, which is similar to the isotope adjustment factors calculated by *Shackleton and Hall* [1984]. This adjustment factor was then applied to the *M. pompilioides* isotope values to produce a continuous isotope data set. The final δ^{18}O curve resembles those at other North Atlantic locations, like ODP Sites 980 and 983 [*Flower et al.*, 2000; *Kleiven et al.*, 2003; *Raymo et al.*, 2004], and IODP Site U1308 [*Hodell et al.*, 2008], and therefore validate the use of *M. pompilioides* at our Site (Figure 2). For the surface water record, we chose to analyze *Neogloboquadrina pachyderma* sin., because this species is present throughout the studied section. A minimum of 15 specimens from the size range between 150 and 250 μm were picked.

[12] Benthic and planktonic specimens of each sample were crushed, ultrasonicated and cleaned with methanol before the isotopic analyses. Benthic and planktonic foraminifer stable isotope analyses were carried out in a Finnigan MAT 252 mass spectrometer at the University of Barcelona. Calibration to the Vienna Pee Dee Belemnite (VPDB) standard scale [*Coplen*, 1996] was made through the NBS-19 standard, and the analytical precision was better than 0.06‰ for δ^{18}O and 0.02‰ for δ^{13}C.

[13] Finally, in order to unravel the dominant frequencies of the Early Pleistocene climate, more specifically for the

Table 1. Tie Points Used in the Correlation Between Benthic δ^{18}O From Site U1314 and Benthic Isotope Stack LR04

Site U1314 Depth (mcd)	LR04 Time (ka)
60.10	780.619
61.79	795.244
62.16	807.358
63.12	817.649
68.55	858.636
68.92	872.225
70.99	921.458
71.88	929.571
75.01	951.451
75.50	962.858
77.60	987.871
79.41	1004.220
83.37	1058.727

time-slice from MIS 31 to 26 (1069–950 ka), we applied a power spectral methodology to five different time series; benthic and planktonic oxygen record, IRD/g and faunal-based SST estimations. Standard time series analysis for these records was carried out using the Lomb periodogram algorithm from the REDFIT module included in *PAST* program [*Hammer et al.*, 2001]. More significant frequencies were determined using the 99%, 95% and the 90% false-alarm levels from a chi-square distribution.

4. Age Model

[14] We converted depth to age matching the distinct glacial and interglacial periods in Site U1314 according to the benthic δ^{18}O record with their temporal equivalent in the orbitally tuned benthic isotope stack of *Lisiecki and Raymo* [2005] (hereinafter referred to as LR04) by using *AnalySeries* 2.0 software [*Paillard and Yiou*, 1996]. Two magnetostratigraphic events corroborate the age model: the Brunhes-Matuyama boundary (780 ka) was identified at 60 mcd in Site U1314 [*Channell et al.*, 2006] and correlates to MIS 19 in the oxygen isotopic record (Figure 2). However, the age of the Brunhes-Matuyama transition is still controversial depending on the method used to measure the mean point of the transition [*Channell et al.*, 2010]. The top of the Jaramillo (990 ka) was placed at 77.7 mcd and correlates with MIS 27.

[15] The final age model for the 24.16 m studied section spans an interval of ~290 kyr through the Early and Mid-Pleistocene based on 13 stratigraphic tie points (Table 1), yielding a temporal resolution of ~0.5 kyr. In between the tie points, sedimentation rates were assumed constant and the ages were deduced by linear interpolation. The orbitally tuned age model and corresponding linear sedimentation rates are shown in Figure 2. The resulting sedimentation rates are moderately high (average 9.3 cm/kyr) and differ largely between glacial (1.15 cm/kyr) and interglacial (up to 27 cm/kyr), intervals indicating enhanced the Gardar Drift growth during intervals of warmer climate. According to our geochronology, the average age resolution is of 230 years per sample (range: ~70 to 600 years) and 1140 years (range: ~365 to 3000 years) for sample interval. The δ^{18}O records from sites 980, 983, U1313 and U1308 (Table 2) are all plotted versus age in Figure 3, using their respective original chronologies in order to see the similarity between the age

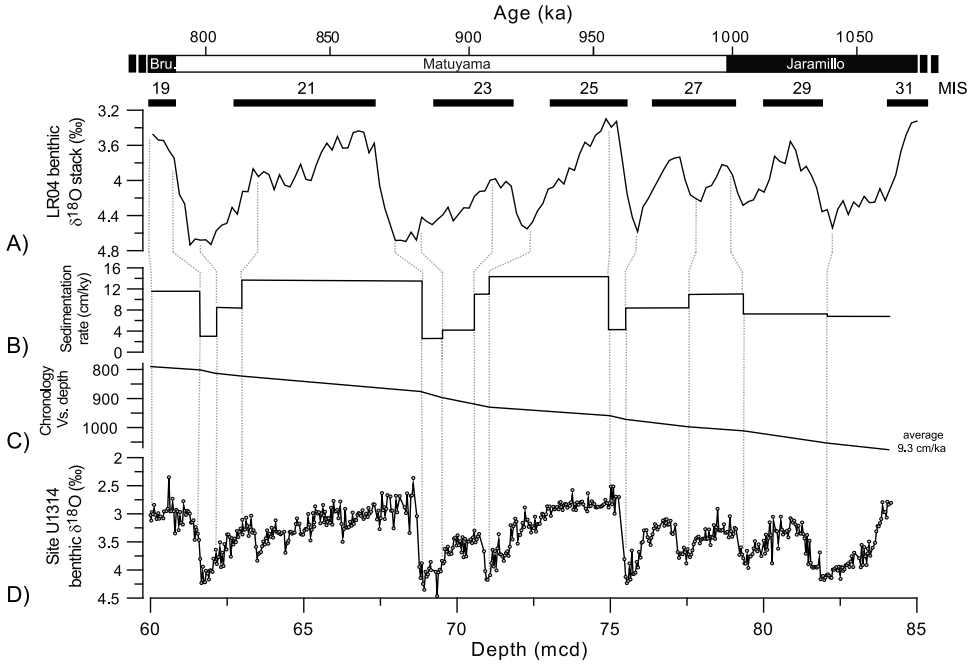

Figure 2. Construction of the age model was performed by correlating the benthic isotope stack LR04 with Site U1314 benthic δ^{18}O. Tie points of both records are joined by dashed lines. From top to bottom: (a) LR04 benthic stack; (b) sedimentation rate of Site U1314 after tuning; (c) chronology as a function of depth in Site U1314; and (d) benthic δ^{18}O from Site U1314 as function of depth. Interglacial stages are shown at the top, in black. Upper bar indicates the magnetic polarity zones (black normal and white reverse).

Table 2. Site Information

Site	Latitude	Longitude	Depth (m)	Reference
U1314	56°36′N	27°88′W	2820	this study
980	55°29′N	14°42′W	2168	*Flower et al.* [2000]
983	60°23′N	23°38′W	1985	*Kleiven et al.* [2003]
U1308	19°53′N	24°14′W	3872	*Hodell et al.* [2008]
U1313	41°00′N	35°58′W	3426	*Ferretti et al.* [2010]

models of each record. Graphic correlation was based on the orbital and suborbital patterns, with the dashed lines joining same events identified in the respective benthic δ^{18}O records (Figure 3).

5. Results

5.1. Oxygen Isotopes

[16] The benthic oxygen isotope record from Site U1314 tuned to LR04 time scale spans six different climate cycles G-IG cycles (from MIS 31 to MIS 19) (Figure 2). From MIS 31 to 22, each glacial/interglacial cycle has an average duration around 41 kyr, while MIS 21 show a longer duration cycle (80 kyr) broken into four interstadial periods. The benthic δ^{18}O data at Site U1314 ranges between 4.45‰ at 882 ka and 2.34‰ at 784 ka (Figures 3d and 4b). Between 1069 and 950 ka (MIS 31–25), the amplitude of oxygen isotope change between glacial and interglacial intervals rarely exceeded 1‰ (only MIS 25/26 transition, with 1.7‰). This trend ends abruptly after MIS 24, with a noticeable shift toward higher benthic δ^{18}O and G-IG amplitude of ~1.8‰. Superimposed on this orbitally related long-term trend, we observe rapid and shorter (in magnitude and duration) oscillations in the δ^{18}O record (planktonic and benthic) (Figures 4b and 4c). A clear example is the four abrupt cooling events that interrupted the warm MIS 21 period, with fluctuations in the planktonic record that exceed 1‰ (Figure 4c). Also it is noticeable that no large IRD peaks occur when benthic δ^{18}O is less than 3.5‰; these periods are characterized by a relative stability without any major IRD discharge event (Figure 4f).

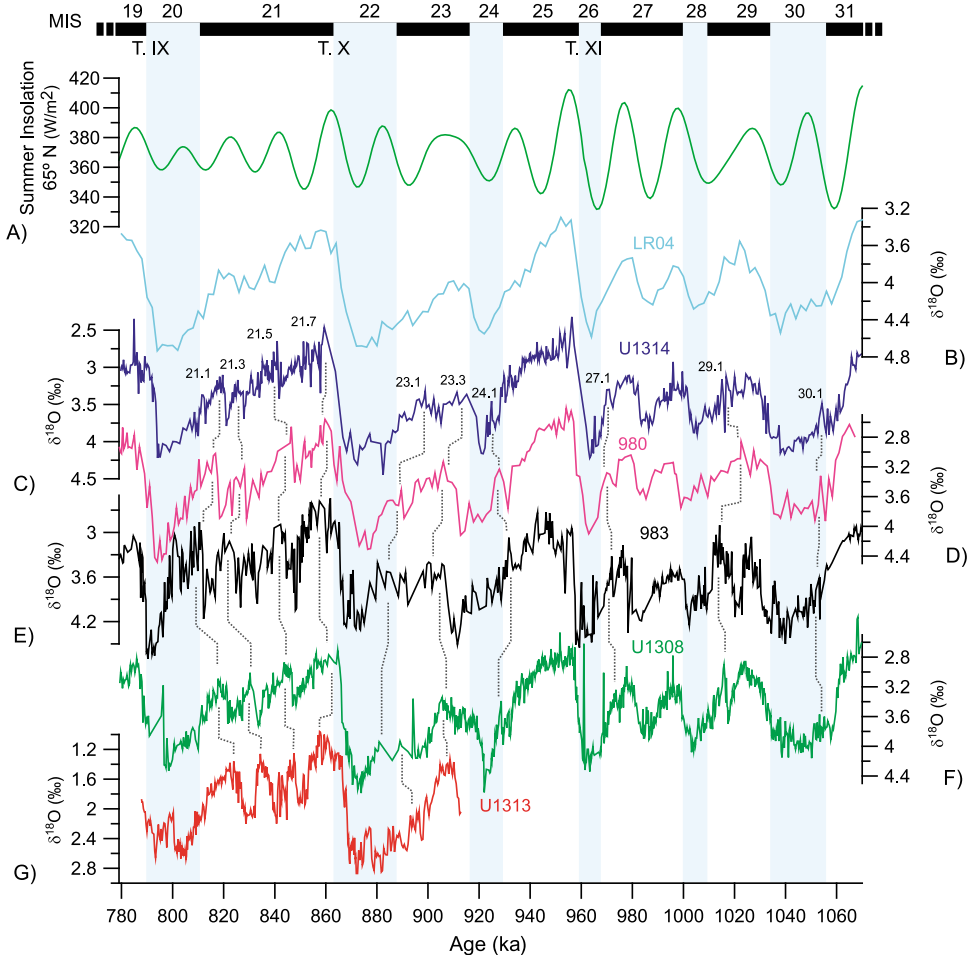

Figure 3. Comparison of benthic δ^{18}O records from the North Atlantic. From top to bottom: (a) summer insolation 65°N [*Laskar et al.*, 2004]; (b) benthic δ^{18}O LR04 stack [*Lisiecki and Raymo*, 2005]; (c) U1314; (d) 980 [*Flower et al.*, 2000]; (e) 983 [*Kleiven et al.*, 2003]; (f) U1308 [*Hodell et al.*, 2008]; and (g) U1313 [*Ferretti et al.*, 2010]. Vertical dashed gray lines join equivalent millennial-climate events in the North Atlantic sites. Marine Isotope Stages (MIS) are shown at the top (glacials in blue, and vertical blue bars, and interglacials in black). Terminations are indicated with roman numbers from XI to IX.

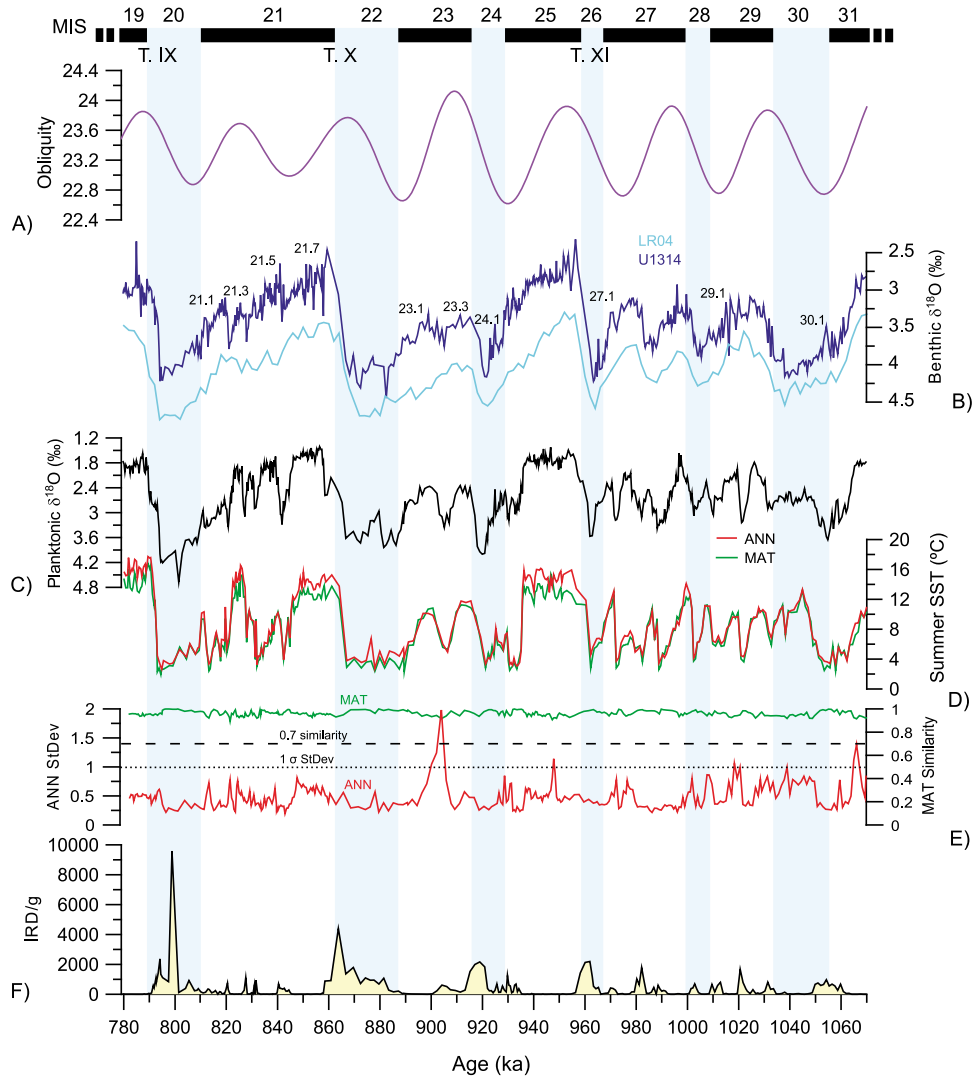

Figure 4. Site U1314 records from 779 to 1069 ka. From top to bottom: (a) obliquity [*Laskar et al.*, 2004]; (b) benthic δ^{18}O (dark blue), benthic δ^{18}O LR04 stack [*Lisiecki and Raymo*, 2005] (light blue); (c) planktonic δ^{18}O; (d) faunal-based SST, using MAT (green) and ANN (red); (e) similarity index of MAT (dashed line) and standard deviation of ANN (dotted line); and (f) IRD/g. Vertical gray bars indicate IRD discharge events, either linked to deglaciations or to millennial-scale oscillations. Marine Isotope Stages (MIS) are shown at the top (glacials in blue, and vertical blue bars, and interglacials in black). Terminations are indicated with roman numbers from XI to IX.

5.2. Faunal-Based Sea Surface Temperatures

[17] Summer SSTs calculated with ANN and MAT techniques are very similar, with the exception of peaks during MIS 25, 21.7 and 19, where ANN estimates suggest higher temperatures up to 2°C higher than MAT (Figure 4d). The generalized low StDev values and the similarity index over 0.7 (Figure 4e), indicate that the studied samples are well represented in the modern data set and the SST estimates provide a faithful trend reconstruction, supported by the similarity of the curves to that of the planktonic δ^{18}O record. Only a few samples from ANN reconstructions are affected by no-analog situations, as indicated by ANN StDev larger than 1σ [*Kucera et al.*, 2005]. These no-analog situations occur within temperate intervals, when planktonic foraminifer assemblage is dominated by *N. pachyderma* sin. and *G. inflata*, with low percentages of *N. pachyderma* dex., an unusual assemblage with no present-day analog in the MARGO Atlantic database.

[18] SST estimates range between 17.1 and 2.3°C. Modern SST values for Site U1314 at 10 m depth are around 12°C [*Locarnini et al.*, 2006], which is in the range of the mean summer SST from ANN and MAT techniques for the interglacial periods before MIS 26, but considerably lower, by more than 4°C, after MIS 25 (Figure 4d). Although the minimum SST does not vary considerably throughout the studied section, slightly colder temperatures are recorded at glacial maxima of MIS 22 and 20. Paleotemperature estimates indicate that G-IG variability shifted to higher amplitude changes after MIS 25, ranging between 4 and 12°C. Moreover, frequent SST oscillations are seen on short timescales throughout the MIS 31 to MIS 19 interval, SST minima always coinciding with IRD discharges.

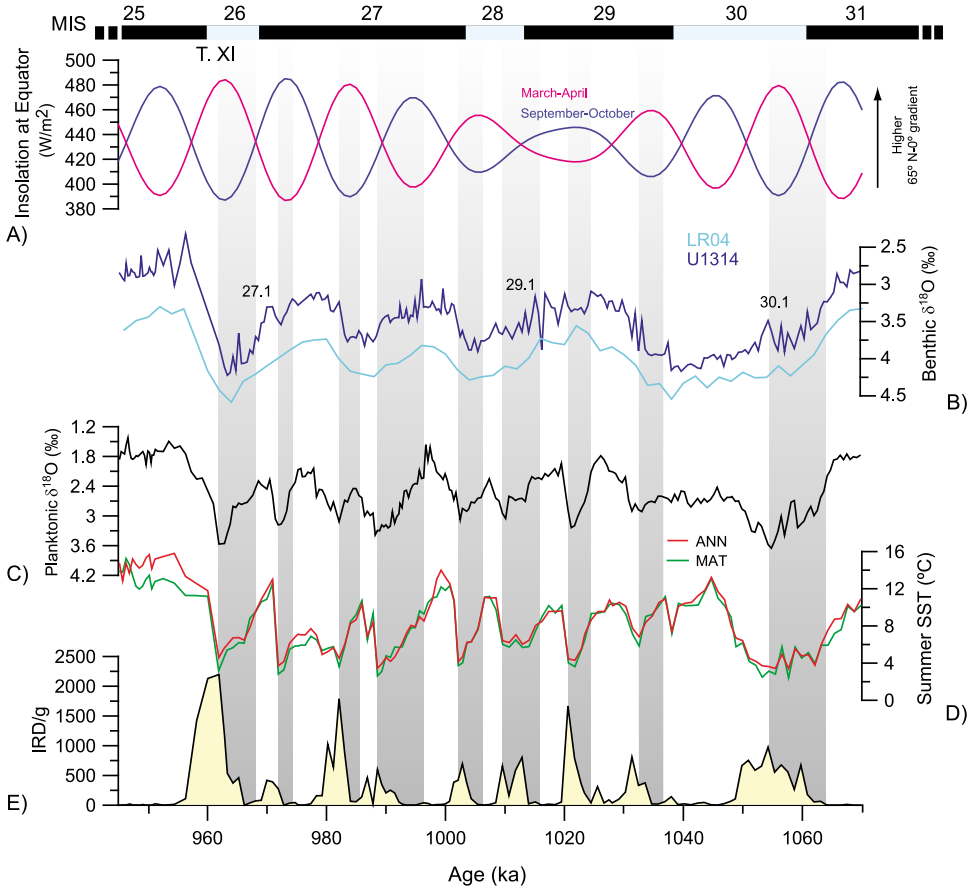

Figure 5. Site U1314 records between 1069 and 950 ka. From top to bottom: (a) insolation at the Equator in Spring (orange solid line) and Autumn (blue dashed line) [*Laskar et al.*, 2004]; (b) benthic δ^{18}O (dark blue), benthic δ^{18}O LR04 stack [*Lisiecki and Raymo*, 2005] (light blue); (c) planktonic δ^{18}O; (d) faunal-based SST, using MAT (green) and ANN (red) technique; and (e) IRD/g. Vertical gray bars indicate SST decreasing phase. Marine Isotope Stages (MIS) are shown at the top (glacials in blue and interglacials in black). Marine Isotope Stages (MIS) are shown at the top (glacials in blue, and vertical blue bars, and interglacials in black). Terminations are indicated with roman numbers from XI to IX.

5.3. Ice-Rafted Debris

[19] IRD were deposited at Gardar Drift mainly during glacial cycles (i.e., MIS 20, 22, 24, 26, 28 and 30) (Figure 4f) exhibiting a saw-tooth steadily upward increase. All iceberg episodes occur when benthic δ^{18}O values surpass values of 3.5‰. The largest IRD events occurred at glacial Terminations 24/23, 22/21 and 20/19 and lithic discharge maximum occurred near the mid-point of the deglacial interval, as defined by the δ^{18}O record. There is a common feature in the IRD record, the planktonic δ^{18}O and SST signals; between MIS 31 and MIS 25, there are nine millennial-scale climate events with an average period of 10 kyr with the peaks of IRD occurring between the transition from the maximum cooling to the subsequent warming, as depicted in the SST and planktonic δ^{18}O records (Figures 5c and 5e). We also observe a steady rise in the magnitude of the IRD events toward more recent stages. In contrast, little IRD input occurs during the peak interglacial maxima of MIS 19, 21, 23, 25, 27 and 29, although several IRD are located at cooler interglacial sub-stages, such as within MIS 21, 27 and 29 (Figure 4f). A notable increase in the glacial input of ice-rafted material occurred at Site U1314 since MIS 24 (~930 ka). The input of ice-rafted terrigenous material during this glacial period and the following glaciations was higher and lasted longer when compared to the previous glacial intervals e.g., MIS 26–30. Maximum IRD input occurs during MIS 20 made up of two distinct peaks (at 794 and 798 ka), that reached accumulations of about 18,000 particles cm^{-2} kyr^{-1}. The ice-rafted debris is mainly composed of quartz and volcanic glass, as well as lithic grains of volcanic, plutonic and metamorphic rocks. Overall, peaks in quartz occur together to high amounts of volcanic glass No detrital carbonate was observed in the coarse fraction.

5.4. Time Series Analysis

[20] The observed high-frequency climate events in the IRD, SST and planktonic δ^{18}O time series (Figures 5c–5e) suggest the existence of a higher-frequency component controlling these records. As they have been detected in the time domain, we performed a time series analysis on IRD, SST and planktonic δ^{18}O records for the time slices before MIS 25 (1069–950 ka) to corroborate this observation. As

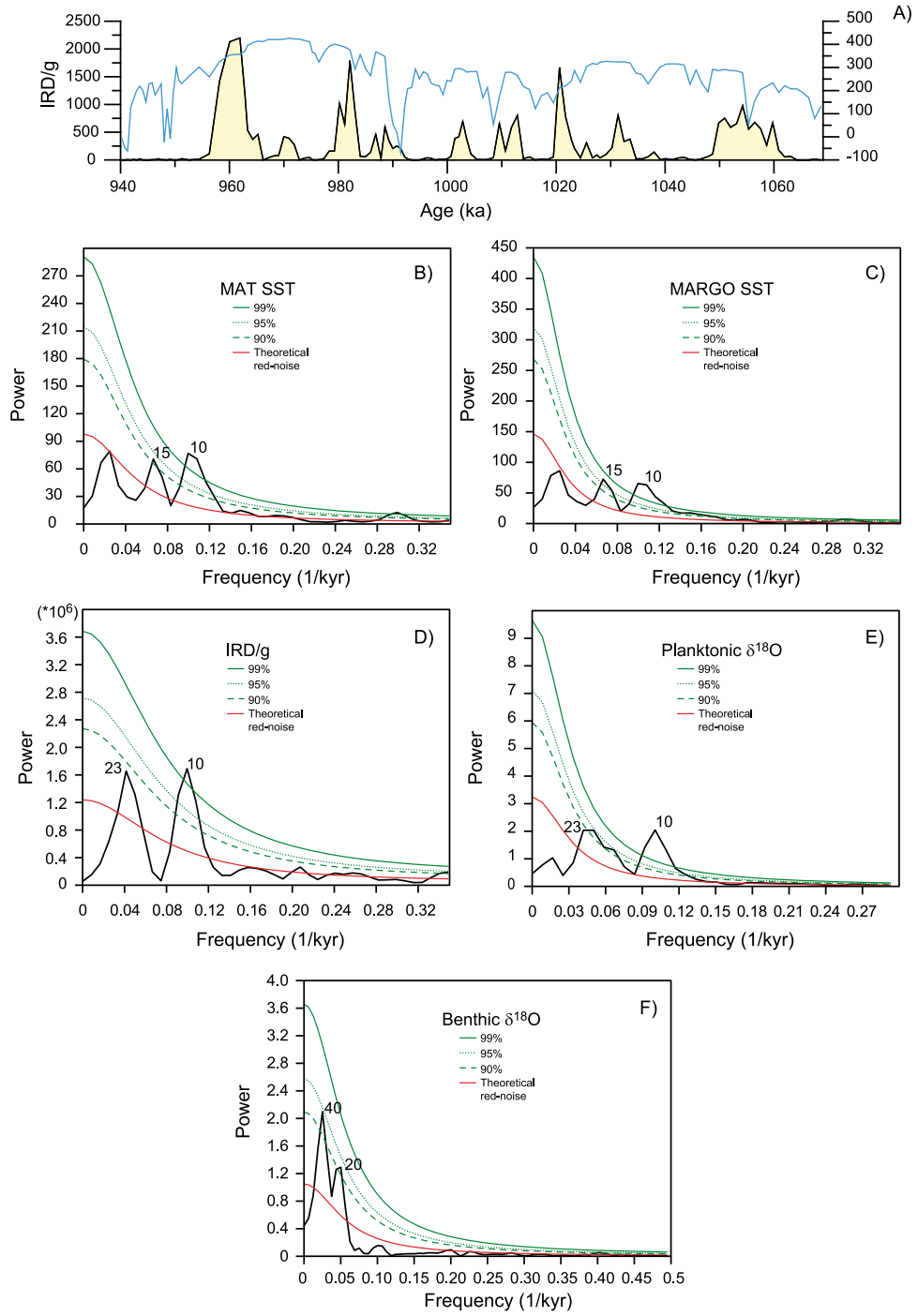

Figure 6. (a) IRD/g record (yellow) for the interval 1069–950 ka and high-pass filtered (blue) to eliminate low-frequency (Milankovitch band) variations. Spectral analyses of Site U1314 records for the same interval (before MIS 25): (b) MAT SST; (c) MARGO SST; (d) IRD/g; (e) Planktonic δ^{18}O; and (f) Benthic δ^{18}O. Spectra were calculated using the Lomb periodogram method with Welch taper. The green lines respectively indicate the 99%, 95% and the 90% false-alarm levels from a chi-square distribution. The red line indicates the AR(1) theoretical red-noise spectrum. Peaks exceeding the false-alarm level indicate non-AR(1) components in a time series, being considered significant, and labeled by period in kyr. The spectrums were obtained by a REDFIT module included in *PAST* program [*Hammer et al.*, 2001].

the IRD/g record is 'clipped' (nonzero values with only positive excursions above the mean), high frequency variability can be an artifact of the sharp transitions introduced by the clipping [*Hagelberg et al.*, 1994]. In order to isolate the higher frequencies, the IRD data were high-pass filtered to exclude the lower frequencies associated with the Milankovitch band (Figure 6a). We observe significant high-frequency oscillations at periods shorter than precession, and

hence validate the results obtained in the spectral analyses (Figure 6d).

[21] Results show dominant periodicities on orbital and suborbital timescales (Figures 6b–6e). The IRD and the planktonic $\delta^{18}O$ lack long-term orbital frequencies of 100 and 41-kyr, and show pronounced spectral peaks at 23 and 10-kyr. The SST signal contains two peaks at 15 and 10-kyr. We also performed spectral analyses on the benthic $\delta^{18}O$ record, which shows longer-frequency 40 and 20-kyr peaks (Figure 6f).

6. Discussion

[22] The MPT, the period between 940 and 900 ka (MIS 25–23), has been associated with a global increase in ice-volume related to a major change in frequency of the climate cycles that evolved from 41-kyr to 100-kyr [e.g., *Mudelsee and Stattegger*, 1997; *Mudelsee and Schulz*, 1997; *Pisias and Moore*, 1981; *Prell*, 1982]. This bifurcation in the climate system is clearly seen in the benthic $\delta^{18}O$ record at Site U1314 along with other proxies (Figure 4b), and reflects a shifting environment toward more extreme glacial conditions and greater G-IG contrast that characterizes the Earth's climate during the Late Pleistocene. Due to the changing structure of climate cycles during the MPT, we have divided our studied interval into two different time-slices in order to discuss the millennial-scale climate oscillations in the North Atlantic.

6.1. Period Between MIS 31 and MIS 26: Low Amplitude, Obliquity and Precession-Driven G-IG Variability

[23] This period immediately predates the onset of the high amplitude 100-kyr G-IG cycles that characterizes climate changes during the Late Pleistocene [*Imbrie et al.*, 1993]. Whereas ice sheet dynamics as recorded by the benthic $\delta^{18}O$ values is mainly driven by precession and obliquity, hydrographic changes of North Atlantic surface waters typically display a suborbital variability dominated by a 10-kyr period (Figures 5c–5e). Glacial stages depict a symmetrical pattern, with similar gradual patterns of glacial growth and deglaciations (Figure 5b).

[24] Based on the high abundance of quartz in the IRD layers at Site U1314, we proposed Scandinavian and Greenland ice sheets as sources for these detrital grains [*Grousset et al.*, 1993]. The presence of volcanic materials implies input from the Icelandic area. Since the largest sand-sized shards cannot be transported by wind, they must be ice-rafted [*Grousset et al.*, 1993; *Ruddiman and Glover*, 1972]. The absence of detrital carbonate in the coarse fraction samples discards any partial input from Canadian icebergs to Site U1314 before 779 ka, as demonstrated by *Hodell et al.* [2008] for Site U1308. However, in our study is difficult to assess this only based in coarse lithic grains, and more accurate analysis are needed to confirm our results.

[25] SST at Site U1314 cyclically vary between high (14°C) and low temperatures (10–4°C), leading to nine millennial-scale climate cycles paced every 10-kyr (Figure 5d). Observed surface water variations with millennial-scale shifts between warmer and colder conditions suggest high-frequency changes in the positioning of the AF. This observation would be consistent with the presence of relatively cool and fresh arctic surface waters, with seasonal sea-ice cover [*Sarnthein et al.*, 2003]. Each of these cycles starts with an abrupt warming event that is followed by gradual and progressive cooling to culminate with an event of iceberg discharge at the time of maximum cooling or the ensuing prominent warming. As has been proposed for climate oscillations in MIS 3, IRD events can be linked with iceberg discharges associated with episodes of ice sheet advance toward the coastline at times of maximum cooling [*Marshall and Koutnik*, 2006], whereas the ensuing warming events are related to minor episodes of ice sheet retreat that can be seen in other records all over the North Atlantic (Figures 3c–3g). In particular, some of the most prominent millennial-scale warmings and the associated IRD events that precede them are clearly linked to ice sheet decay and global decreases in ice-volume as they coincide with deglaciations at transitions between MIS 30/29, MIS 28/27, and the large deglaciation at Termination XI, between MIS 26/25 (Figures 5b–5e), that is the most prominent IRD event and signal the onset of the 100-kyr cycles of the Late Pleistocene. In the same way, the warming events not associated with major deglaciations usually take place at times of apparent interruptions of ice growth or even minor decreases in ice-volume as they usually take place at times of short inversions in the otherwise increasing benthic $\delta^{18}O$ values (Figure 5b). This pattern of minor global sea level rises is very evident at least during some of the 'so-called Bond cycles' of MIS 3, in which sea level rises on the order of 10 to 30 m have been associated either to the IRD events (Heinrich events) or to the prominent warming events that follow them [*Arz et al.*, 2007; *Siddall et al.*, 2003; *Sierro et al.*, 2009]. A clear exception to this pattern is observed in MIS 27.1, although almost no IRD event is recorded during this period, the warming event is not linked to ice decay but to a short event of rapid ice growth during this substage.

[26] In order to check if these minor episodes of ice sheet retreat are recorded in other North Atlantic benthic oxygen isotope records we compared our benthic isotope record with previously published results from Sites 980 [*Raymo et al.*, 2004], 983 [*Kleiven et al.*, 2003], U1308 [*Hodell et al.*, 2008], and with U1313 for the time interval over which these two records overlap (910–790 ka) [*Ferretti et al.*, 2010]. Figure 3 show the established correlation of the negative oxygen isotope excursions between all Sites, while climate events MIS 30.1 and 21.1 can also be observed in LR04 record despite the lower resolution of these signals. We argue that the ^{18}O depletions observed at the base of these millennial-scale climate changes can be partially related to low amplitude rises in sea level similarly to those observed during the Bond cycles [*Arz et al.*, 2007; *Siddall et al.*, 2003; *Sierro et al.*, 2009]. However, the regional occurrence of these negative oxygen isotope excursions all over the North Atlantic does not necessarily prove they are caused by ice-volume decreases, since there are no independent records of sea level for this time to test this hypothesis. Instead, we suggest that these ^{18}O depletions were probably amplified by the deep water hydrographic change. In some cases the magnitude of these negative oxygen isotope anomalies is in the order of 0.7‰ (e.g., MIS 21.5 and 21.1) that is too high to be only associated with ice-volume since this would represent eustatic sea level increases of 40–70 m. Consequently, we hypothesize that besides

the influence of sea level, millennial-scale changes in benthic $\delta^{18}O$ partially resulted from the influence of southern water masses (LDW) in the North Atlantic basin with different temperature and salinity [*Skinner et al.*, 2003], or isotopically light water generated by brine formation in the GIN Seas [*Dokken and Jansen*, 1999; *Vidal et al.*, 1998].

6.2. Period Between MIS 25 and MIS 19: Higher Amplitude Ice-Volume Changes

[27] It is in MIS 25 when the typical configuration of the 100-kyr glacial cycles is initiated; the first two cycles are recognized in this work from MIS 25 to MIS 22 with a duration of ~100-kyr and from MIS 21 to MIS 19 that only lasted ~80-kyr (Figure 4b). Since MIS 25, we observe a positive shift in benthic $\delta^{18}O$ during glacial stages and greater G-IG amplitude variability, generally ascribed to continental ice sheet expansion and to more severe glaciations [*Berger et al.*, 1999; *Pisias and Moore*, 1981], and more G-IG contrast in surface water proxies, planktonic $\delta^{18}O$ values and SST, in a way similar to the ice-volume variations [*Lisiecki and Raymo*, 2005]. The amplitude of G-IG change in planktonic $\delta^{18}O$ and faunal-based SST increased at MIS 25, with shifts of ~2.5‰ and ~12°C, respectively, and with interglacial temperatures over 16°C at MIS 21 and 19 (Figures 4c and 4d). We interpret this as a greater northward retreat of the AF to a more northerly position during interglacials than that experienced during the previous time interval. Based on faunal data from sites 980 and 984, and percentage of $C_{37:4}$ alkenone from Site 983, several authors documented a similar change in surface water conditions toward higher G-IG contrast after MIS 25 [*McClymont et al.*, 2008; *Wright and Flower*, 2002]. This greater G-IG variability might have acted as a positive feedback by increasing the latitudinal temperature gradient that drives moisture transport to the high latitudes, and thus promoting the growth of larger ice sheets than in the preceding time interval. The expansion of Northern Hemisphere ice sheets altered the patterns of glacial growth and deglacial decay producing a more asymmetric response. Glacial progressions after MIS 25 are considerably longer than the previous glacial periods due to the new configuration of climate cycles.

[28] We observe an amplification of the magnitude and duration of IRD events after MIS 25 respect to the previous period (Figure 4f) that correlates with the documented increased IRD deposition along the Norwegian-Greenland margins and Barents Sea after 900 ka [*Helmke et al.*, 2003; *Henrich and Baumann*, 1994; *Jansen et al.*, 1988; *Knies et al.*, 2009]. The increased abundance of IRD would be attributed to a pronounced ice sheet expansion in the circum-Atlantic region, reaching fully development in thickness and height already during the Early Pleistocene [*Knies et al.*, 2009; *Sejrup et al.*, 2000]. Larger ice sheet growth would be consistent with our hypothesis that increased moisture transport to high latitudes after MIS 25 contributed to the development of more extensive ice sheets. Increased northward flow of warmer waters during MIS 25, 21 and 19 increased heat transport to the region (Figure 4d). Warm water into the GIN Seas would have led to increase evaporation and precipitation, thus providing a positive feedback for ice sheet growth [*Hebbeln et al.*, 1994; *Ruddiman and McIntyre*, 1979]. This mechanism is compatible with paleoclimatic data and models that assume that ice-volume growth during MPT augmented bed-rock depression, leading to more unstable ice sheets that fully melted during interglacial periods [*Clark and Pollard*, 1998].

6.2.1. Climate Cycle From MIS 25 to MIS 21

[29] Following MIS 25 that marks the onset of this ~100 kyr climate cycle, ice sheet growth was only punctuated by some short events of lower ice-volume and a major interglacial at MIS 23.3, but the amplitude of this interglacial period was lower than that recorded during interglacial periods before MIS 25 (Figure 5b). Consequently, this climate cycle is in fact composed of two obliquity-driven climate cycles with glacial phases at MIS 24 and MIS 22 and the deglaciation of MIS 23.3 probably triggered by the prominent maximum in obliquity at that time (Figure 4a).

[30] During the pronounced interglacial period at MIS 25 SST remained high at around 14°C for a long period of time spanning between 956 and 935 ka (Figure 4d). During this time period ice-volume was low or slightly increasing, however, a sharp and prominent cooling of surface waters that changed from 15 to 3°C in only 2 kyr, marks the onset of rapid ice sheet growth as illustrated by the increase in the benthic $\delta^{18}O$ record (Figure 4b). Accumulation of ice on the continents is clearly linked to a rapid southward migration of the AF at the latitude of Site U1314 and is followed in only a few kiloyears by iceberg discharge.

[31] Three short climate events were recorded during the glacial period of this climate cycle, a short, low amplitude warming event at the transition between MIS 25/24 (MIS 24.1), and two more prominent warming events at MIS 23.3 and MIS 23.1. All three events are paced by ~14 ka, and describe same warmer SST-cooling-IRD discharge event related to ice sheet decay events that can be seen in other North Atlantic benthic $\delta^{18}O$ records (Figures 3c–3g).

6.2.2. Climate Cycle From MIS 21 to MIS 19

[32] This period is characterized by the presence of two prominent warming events at MIS 19 and 21, following the first major expansion of polar ice sheets at MIS 22 [*Head and Gibbard*, 2005]. This climate cycle starts with an abrupt increase in SST at Termination X that pass from 4 to 14°C in only 6 kyr (MIS 21.7) resulting in a rapid collapse of the ice sheets that is recorded by a pronounced increase in the IRD/g (Figure 4f). Surface ocean conditions during MIS 21.7 were typical of interglacial maxima of the Late Pleistocene, with low-ice volume and no IRD discharges, which were interrupted at 842 ka with an abrupt shift toward heavier benthic $\delta^{18}O$ values.

[33] During the subsequent section, between substage 21.7 to Termination IX, three prominent millennial-scale climate oscillations, labeled as 21.5, 21.3, 21.1, are recorded in the faunal derived SST, planktonic oxygen isotopes and the benthic oxygen (Figures 4b–4d). Similarly to that observed in the previous cycles, we observe the same sequence of rapid shifts in temperature that characterizes these millennial climate events (Figures 4b and 4d). These climate fluctuations correspond with substages MIS 21.5, 21.3, 21.1 first described by *Ferretti et al.* [2010] (Figure 3g). These fluctuations in the benthic $\delta^{18}O$ are also visible in all North Atlantic benthic $\delta^{18}O$ records, and at least the northernmost records typically show an asymmetric pattern, with an abrupt decrease in the $\delta^{18}O$ values at the base followed by a gradual increase in $\delta^{18}O$. In the southernmost record (Site U1313)

this pattern is less evident (Figures 3f and 3g). The decrease of δ^{18}O values at the base of millennial fluctuations 21.5, 21.3 and 21.1, as discussed for the interval between MIS 31–26, may be related to low amplitude sea level rises due to smaller ice sheets, deep water warming or a higher influence of the low δ^{18}O southern deep water [*Sierro et al.*, 2009; *Skinner et al.*, 2003].

[34] The increasing discharge of icebergs during the millennial events seems to support the model results reported by *Marshall and Koutnik* [2006]. Similarly as it was proposed by previous authors, we interpret increasing IRD content in the sediments reflects the advance of circum-North Atlantic ice sheet margins toward the shelf-break, resulting in high delivery of icebergs due to calving. Increased supply of moisture from low latitudes during equinox insolation maxima [*Ferretti et al.*, 2010] would promote a positive mass balance in the ice sheets with the consequent gradual sea level drop. Similarly to model results, maximum delivery of icebergs is reached immediately after maximum cooling, during the phase of abrupt warming. *Marshall and Koutnik* [2006] found that peak iceberg flux lags maximum cooling because ice margins kept advancing to the coast 600 years after peak cooling. During the warm phase of the climate oscillations ice margins withdraw from the coast due to ice melting under warmer summer temperatures and no icebergs were delivered to the ocean.

[35] It is worthy to mention that the ice-volume decrease at MIS 21.1 lags obliquity maximum in 6 kyr (Figures 4a and 4b), which is the assumed lag in obliquity during the Pleistocene [*Lisiecki and Raymo*, 2005]. However, this event, which is clearly visible in the benthic δ^{18}O record, is hardly distinguishable in the surface proxies, with only a small increase in SST and a low amplitude decrease in the planktonic δ^{18}O values (Figures 4c and 4d). In contrast, a prominent increase in SST and a decrease in the planktonic δ^{18}O are recorded in MIS 21.3 exactly at the timing of the prominent obliquity maximum. Consequently, an evident lag between maximum temperature at Site U1314 and decreasing ice-volume is recorded in this period, with the temperature changing with obliquity. However, comparing the magnitude of events MIS 21.3 and 21.1 in the other North Atlantic records, we observe that at northern and shallower sites (U1314, 980 and 983), MIS 21.1 is greater than MIS 21.3 (Figures 3c–3e), while at southern and deeper sites (U1308 and U1313) they are similar (Figures 3f and 3g). This could be related to some hydrographic change restricted to the depths and latitudes of the sites U1314, 980 and 983.

6.3. Origin of the Millennial-Scale Climate Changes

[36] As observed in Figure 6 spectral power in the sea surface proxies, SST, IRD and planktonic δ^{18}O, is mainly concentrated on the 10-kyr periodicity, whereas global ice-volume as recorded by the benthic δ^{18}O records shows dominant periods at around 20 and 40 kyr. It is important to note the similarity between the timing of these events at Site U1314 and the millennial-scale variability of massive ice discharges seen in the Late Pleistocene sediments [e.g., *Bond et al.*, 1993; *Heinrich*, 1988; *McManus et al.*, 1999]. One might expect that these high-frequencies did not appear at older sedimentary sequences, owing to the smaller size of the Northern Hemisphere ice sheets, however, an increasing number of marine and terrestrial records at mid-and-high latitudes contain such precessional periodicity and its harmonics during the Early and Mid-Pleistocene [*Bartoli et al.*, 2006; *Grützner and Higgins*, 2010; *Ortiz et al.*, 1999; *Raymo et al.*, 1998; *Wara et al.*, 2000; *Weirauch et al.*, 2008] and during the Pliocene [*Becker et al.*, 2005; *Larrasoaña et al.*, 2003; *Niemitz and Billups*, 2005; *Steenbrink et al.*, 2003; *Willis et al.*, 1999], evidencing that continental ice sheets have oscillated in a similar manner in both the 41-kyr and 100-kyr worlds. Hence, the climatic variability represented by surface proxies at Site U1314 might be driven by some component of the system that is consistent throughout the Pleistocene, well before the Northern Hemisphere Glaciation (NHG).

[37] The 23-kyr rhythm and its harmonics are very strong in low latitudes up to 40°N, with power diminishing northward [*Ruddiman and McIntyre*, 1981; *Ruddiman and McIntyre*, 1984]. The precessional-related cyclicity is present in different features of surface oceanography at low-latitudes, including primary productivity proxies and changes in wind intensity related to monsoonal variability [*McIntyre and Molfino*, 1996; *McIntyre et al.*, 1989; *Molfino and McIntyre*, 1990]. The most accepted mechanism that originates this frequency bands at low-latitudes is an external climate forcing attributed to the twice-yearly passage of the sun across the equator during each precession cycle [*Short et al.*, 1991], that generates a signal of half the precession period at the equator. Direct consequence of this process would be the enhanced transport of heat and moisture supply via oceanic and atmospheric circulation from equatorial latitudes to the higher latitudes of the North Atlantic. This mechanism has been invoked to explain the presence of the 10-kyr cycles in oceanic sediments from mid-and-high latitudes in the North Atlantic [*Ferretti et al.*, 2010; *Hagelberg et al.*, 1994; *McIntyre and Molfino*, 1996; *Weirauch et al.*, 2008].

[38] The observation of a prominent 10-kyr variability in our planktonic δ^{18}O, SST and IRD/g record with each equinox at Equator between MIS 31 and MIS 25 (Figures 5a and 5c–5e) led us to speculate that changes in insolation at low latitudes may be responsible for the oceanographic and ice sheet events described in this study. During both equinoxes insolation maxima at equator, the latitudinal gradient between 65°N and 0°N reaches the maximum values, leading to higher atmospheric contrast between high and low latitudes, and thus intensifying atmospheric circulation that results, in turn, in enhanced meridional moisture flux. A higher transport of warm water to the polar regions of the northern hemisphere increases the ice-ocean moisture gradient and accelerates ice sheet growth, and consequently, the larger the ice sheet, the more sensitive it becomes to that excess accumulation. This will result in enhanced ice sheet calving associated to the rapid advance of the ice margins to the coast or the shelf-break [*Marshall and Koutnik*, 2006]. Although speculative, this mechanism would relate the major ice-rafting pulses and surface-deep ocean dynamics to an external forcing originated at low-latitudes.

[39] Sub-Milankovitch variability in the SST estimates ranges from 15 to 10-kyr (Figures 6b and 6c). The longer of these periodicities (15-kyr) did not achieve the 99% of significance in our records. Interpretation of this frequency band of climatic variability outside the direct orbital forcing band may be tentatively explained in terms of the climatic

system's nonlinear response to variations in the insolation. Power at 15-kyr could arise as a roughly combination tones of the obliquity and precession frequencies found in the insolation parameters [*Berger and Pestiaux*, 1984; *Yiou et al.*, 1994]. Hence, the lack of a definite physical interpretation to interpret this signal suggests the need for caution when interpreting the 15-kyr peak as a potential suborbital cyclicity. Additional work is needed to replicate this observation in other records and/or analysis with other spectral methodologies.

[40] The benthic $\delta^{18}O$ record is controlled by the 40-kyr cycle of obliquity and the 20-kyr cycle of precession, whereas a direct influence of the half-precession is notably absent (Figure 6f). This is in contrast to the spectral characteristics of the surface water proxies records (planktonic $\delta^{18}O$, SST and IRD/g) for the same time interval. The change in benthic $\delta^{18}O$ on both obliquity and precession time scales are interpreted to reflect the direct influence of astronomical induced insolation changes on the North Atlantic ice-volume [*Berger et al.*, 1999; *Hays et al.*, 1976]. The absence of a clear half-precession signal in benthic $\delta^{18}O$ record of Site U1314 confirms that this record is not significantly altered by changes in the properties and volume of the inflowing Atlantic surface waters and/or moisture transport to high latitudes, but dominated by global-scale G-IG variations.

7. Conclusions

[41] The high-resolution records at IODP Site U1314 between 1069 and 779 ka provide new insights on the millennial-scale climate variability of the North Atlantic and its impact into circum-Atlantic ice sheets dynamics during the MPT. Cool surface waters but moderate ice-volume characterized the older time-slice (MIS 31–26). The reconstruction of SST through the study of planktonic foraminifer assemblages revealed the occurrence of millennial-scale climate oscillations typically associated to the periods of ice sheet growth. These climate fluctuations are characterized by phases of gradual cooling and enhanced iceberg discharge and culminate with an abrupt warming event. Peaks of maximum IRD content are always linked to maximum cooling of surface waters or the ensuing warming event, supporting recent climate models [*Marshall and Koutnik*, 2006]. Consequently we associated IRD peaks and the iceberg discharges that caused them with episodes of circum-Atlantic ice sheets advance toward the coastline at times of maximum cooling. The lower benthic $\delta^{18}O$ values usually observed at the times of IRD events and the ensuing warming events may be related to low amplitude sea level rises due to ice sheets retreats, to deep water warming or to a higher influence of the low $\delta^{18}O$ southern deep water. Moreover, our IRD data support the hypothesis that the MPT represents a fundamental change in ice sheet dynamics that is consistent with the growth of thicker, more unstable ice sheets that fully melted during interglacial periods [*Clark and Pollard*, 1998].

[42] IRD, SST and planktonic $\delta^{18}O$ time series analysis show a significant concentration of variability at periods of half-precessional cycles (10-kyr), and IRD and planktonic $\delta^{18}O$ also at precessional cycles (23-kyr). The timing and structure of these events suggest that ice surges might be induced by latitudinal export of equatorial insolation forcing to high-latitudes via tropical convective process, either atmospheric or oceanic.

[43] In conclusion, our study outlines the importance of latitudinal energy and moisture gradients and atmosphere-ocean-cryosphere feedback mechanisms to generating and transporting this millennial-scale climate variability globally. Their occurrence at times before the intensification of the NHG evidence that they acted independently of the ice accumulated in continental glaciers. The 15-kyr peak in the SST spectra may indicate the existence of nonlinear response to variations in the insolation. The lack of evidence of 10-kyr periodicity in the benthic $\delta^{18}O$ signal indicates that these high-frequency climate oscillations are only related to surface water proxies.

[44] **Acknowledgments.** This work was funded by Ministerio de Ciencia e Innovación Project GRACCIE (CONSOLIDER-INGENIO CSD 2007–00067), CGL2008–05560/BTE, and CGL2011–26493 as well as by Junta de Castilla y Leon Grupo GR34 and by a MEC FPI Grant to Iván Hernández-Almeida (BES-2006-12787). We are grateful to Montserrat Alonso-García for her help in performing the SST reconstructions and to Øyvind Hammer for his many discussions of spectral analysis. The two anonymous reviewers are acknowledged for their critical evaluation, constructive opinions, and helpful suggestions. We also thank the MARGO organizing committee for providing fauna database from the North Atlantic. This research used samples from IODP Expedition 306.

References

Alonso-Garcia, M., F. J. Sierro, M. Kucera, J. A. Flores, I. Cacho, and N. Andersen (2011), Ocean circulation, ice sheet growth and interhemispheric coupling of millennial climate variability during the mid-Pleistocene (ca 800–400 ka), *Quat. Sci. Rev.*, *30*(23–24), 3234–3247, doi:10.1016/j.quascirev.2011.08.005.

Arz, H. W., F. Lamy, A. Ganopolski, N. Nowaczyk, and J. Pätzold (2007), Dominant Northern Hemisphere climate control over millennial-scale glacial sea-level variability, *Quat. Sci. Rev.*, *26*(3–4), 312–321, doi:10.1016/j.quascirev.2006.07.016.

Barendregt, R. W., and E. Irving (1998), Changes in the extent of North American ice sheets during the late Cenozoic, *Can. J. Earth Sci.*, *35*(5), 504–509, doi:10.1139/e97-126.

Bartoli, G., M. Sarnthein, and M. Weinelt (2006), Late Pliocene millennial-scale climate variability in the northern North Atlantic prior to and after the onset of Northern Hemisphere glaciation, *Paleoceanography*, *21*, PA4205, doi:10.1029/2005PA001185.

Becker, J., L. J. Lourens, F. J. Hilgen, E. van der Laan, T. J. Kouwenhoven, and G.-J. Reichart (2005), Late Pliocene climate variability on Milankovitch to millennial time scales: A high-resolution study of MIS100 from the Mediterranean, *Palaeogeogr. Palaeoclimatol. Palaeoecol.*, *228*(3–4), 338–360, doi:10.1016/j.palaeo.2005.06.020.

Berger, A., and P. Pestiaux (1984), Accuracy and stability of the Quaternary terrestrial insolation, in Milankovitch and Climate: Understanding the Response to Astronomical Forcing, Proceedings of the NATO Advanced Research Workshop, edited by A. Berger et al., pp. 83–112, D. Reidel, Palisades, N. Y.

Berger, A., X. S. Li, and M. F. Loutre (1999), Modelling northern hemisphere ice volume over the last 3 Ma, *Quat. Sci. Rev.*, *18*(1), 1–11, doi:10.1016/S0277-3791(98)00033-X.

Berger, W. H., and E. Jansen (1994), Mid-Pleistocene climate shift: The Nansen connection, in *The Polar Oceans and Ttheir Role in Shaping the Global Environment*, edited by O. M. Johannessen, R. D. Muench, and J. E. Overland, pp. 295–311, AGU, Washington, D.C., doi:10.1029/GM085p0295

Bianchi, G. G., and I. N. McCave (2000), Hydrography and sedimentation under the deep western boundary current on Björn and Gardar Drifts, Iceland Basin, *Mar. Geol.*, *165*(1–4), 137–169, doi:10.1016/S0025-3227(99)00139-5.

Bolton, C. T., P. A. Wilson, I. Bailey, O. Friedrich, C. J. Beer, J. Becker, S. Baranwal, and R. Schiebel (2010), Millennial-scale climate variability in the subpolar North Atlantic Ocean during the late Pliocene, *Paleoceanography*, *25*, PA4218, doi:10.1029/2010PA001951.

Bond, G., et al. (1992), Evidence for massive discharges of icebergs into the North Atlantic ocean during the last glacial period, *Nature*, *360*, 245–249, doi:10.1038/360245a0.

Bond, G., W. Broecker, S. Johnsen, J. McManus, L. Labeyrie, J. Jouzel, and G. Bonani (1993), Correlations between climate records from North Atlantic sediments and Greenland ice, *Nature*, *365*(6442), 143–147, doi:10.1038/365143a0.

Bond, G., W. Showers, M. Cheseby, R. Lotti, P. Almasi, P. deMenocal, P. Priore, H. Cullen, I. Hajdas, and G. Bonani (1997), A Pervasive Millennial-Scale Cycle in North Atlantic Holocene and Glacial Climates, *Science*, *278*(5341), 1257–1266, doi:10.1126/science.278.5341.1257.

Channell, J. E. T., T. Kanamatsu, T. Sato, R. Stein, C. A. Alvarez Zarikian, M. J. Malone, and the Expedition 303/306 Scientists (2006), *Site U1314, in North Atlantic Climate*, *Proc. Integr. Ocean Drill. Program*, *303/306*.

Channell, J. E. T., D. A. Hodell, B. S. Singer, and C. Xuan (2010), Reconciling astrochronological and $^{40}Ar/^{39}Ar$ ages for the Matuyama-Brunhes boundary and late Matuyama Chron, *Geochem. Geophys. Geosyst.*, *11*, Q0AA12, doi:10.1029/2010GC003203.

Clark, P. U., and D. Pollard (1998), Origin of the Middle Pleistocene Transition by ice sheet erosion of regolith, *Paleoceanography*, *13*(1), 1–9, doi:10.1029/97PA02660.

Clark, P. U., D. Archer, D. Pollard, J. D. Blum, J. A. Rial, V. Brovkin, A. C. Mix, N. G. Pisias, and M. Roy (2006), The middle Pleistocene transition: Characteristics, mechanisms, and implications for long-term changes in atmospheric pCO2, *Quat. Sci. Rev.*, *25*(23–24), 3150–3184, doi:10.1016/j.quascirev.2006.07.008.

Conkright, M., et al. (1998), World Ocean Atlas 1998 CD-ROM Data Set Documentation, version 2.0, *Natl. Oceanogr. Data Cent. Internal Rep. 14*, 144 pp., NOAA, Silver Spring, Md.

Coplen, T. B. (1996), More uncertainty than necessary, *Paleoceanography*, *11*(4), 369–370, doi:10.1029/96PA01420.

Corliss, B. H. (1985), Microhabitats of benthic foraminifera within deep-sea sediments, *Nature*, *314*(6010), 435–438, doi:10.1038/314435a0.

Corliss, B. H. (1991), Morphology and microhabitat preferences of benthic foraminifera from the northwest Atlantic Ocean, *Mar. Micropaleontol.*, *17*(3–4), 195–236, doi:10.1016/0377-8398(91)90014-W.

Cortijo, E., L. Labeyrie, M. Elliot, E. Balbon, and N. Tisnerat (2000), Rapid climatic variability of the North Atlantic Ocean and global climate: A focus of the IMAGES program, *Quat. Sci. Rev.*, *19*(1–5), 227–241.

Dokken, T. M., and E. Jansen (1999), Rapid changes in the mechanism of ocean convection during the last glacial period, *Nature*, *401*(6752), 458–461, doi:10.1038/46753.

Duplessy, J.-C., N. J. Shackleton, R. K. Matthews, W. Prell, W. F. Ruddiman, M. Caralp, and C. H. Hendy (1984), $\delta^{13}C$ Record of benthic foraminifera in the last interglacial ocean: Implications for the carbon cycle and the global deep water circulation, *Quat. Res.*, *21*(2), 225–243, doi:10.1016/0033-5894(84)90099-1.

Elliot, M., L. Labeyrie, G. Bond, E. Cortijo, J.-L. Turon, N. Tisnerat, and J.-C. Duplessy (1998), Millennial-Scale iceberg discharges in the Irminger Basin during the Last Glacial period: Relationship with the Heinrich Events and environmental settings, *Paleoceanography*, *13*(5), 433–456, doi:10.1029/98PA01792.

Ferretti, P., N. J. Shackleton, D. Rio, and M. A. Hall (2005), Early Middle Pleistocene deep circulation in the western subtropical Atlantic: Southern Hemisphere modulation of the North Atlantic Ocean, in *Early Middle Pleistocene Transitions: The Land-Ocean Evidence*, edited by M. J. Head and P. L. Gibbard, *Geol. Soc. Spec. Publ.*, *247*, 131–145.

Ferretti, P., S. J. Crowhurst, M. A. Hall, and I. Cacho (2010), North Atlantic millennial-scale climate variability 910 to 790 ka and the role of the equatorial insolation forcing, *Earth Planet. Sci. Lett.*, *293*(1–2), 28–41, doi:10.1016/j.epsl.2010.02.016.

Flower, B. P., D. W. Oppo, J. F. McManus, K. A. Venz, D. A. Hodell, and J. L. Cullen (2000), North Atlantic Intermediate to Deep Water circulation and chemical stratification during the past 1 Myr, *Paleoceanography*, *15*(4), 388–403, doi:10.1029/1999PA000430.

Grousset, F. E., L. Labeyrie, J. A. Sinko, M. Cremer, G. Bond, J. Duprat, E. Cortijo, and S. Huon (1993), Patterns of ice-rafted detritus in the glacial North Atlantic (40–55°N), *Paleoceanography*, *8*(2), 175–192, doi:10.1029/92PA02923.

Grützner, J., and S. M. Higgins (2010), Threshold behaviour of millennial scale variability in deep water hydrography inferred from a 1.1 Ma long record of sediment provenance at the southern Gardar Drift, *Paleoceanography*, *25*, PA4204, doi:10.1029/2009PA001873.

Hagelberg, T. K., G. Bond, and P. deMenocal (1994), Milankovitch band forcing of sub-Milankovitch climate variability during the Pleistocene, *Paleoceanography*, *9*(4), 545–558, doi:10.1029/94PA00443.

Hammer, Ø., D. A. T. Harper, and P. D. Ryan (2001), PAST: Paleontological Statistics software package for education and data analysis, *Palaeontol. Electronica*, *4*(1), 4.

Hayashi, T., M. Ohno, G. Acton, Y. Guyodo, H. F. Evans, T. Kanamatsu, F. Komatsu, and F. Murakami (2010), Millennial-scale iceberg surges after intensification of Northern Hemisphere glaciation, *Geochem. Geophys. Geosyst.*, *11*, Q09Z20, doi:10.1029/2010GC003132.

Hays, J. D., J. Imbrie, and N. J. Shackleton (1976), Variations in Earth's orbit: Pacemaker of ice ages, *Science*, *194*(4270), 1121–1132, doi:10.1126/science.194.4270.1121.

Head, M. J., and P. L. Gibbard (2005), *Early Middle Pleistocene Transitions: The Land-Ocean Evidence*, 321 pp., Geol. Soc., London.

Hebbeln, D., T. Dokken, E. S. Andersen, M. Hald, and A. Elverhoi (1994), Moisture supply for northern ice-sheet growth during the Last Glacial Maximum, *Nature*, *370*(6488), 357–360, doi:10.1038/370357a0.

Heinrich, H. (1988), Origin and consequences of cyclic ice rafting in the Northeast Atlantic Ocean during the past 130,000 years, *Quat. Res.*, *29*(2), 142–152, doi:10.1016/0033-5894(88)90057-9.

Helmke, J. P., H. A. Bauch, and H. Erlenkeuser (2003), Development of glacial and interglacial conditions in the Nordic seas between 1.5 and 0.35 Ma, *Quat. Sci. Rev.*, *22*(15–17), 1717–1728, doi:10.1016/S0277-3791(03)00126-4.

Henrich, R., and K. H. Baumann (1994), Evolution of the Norwegian Current and the Scandinavian Ice Sheets during the past 2.6 m.y.: Evidence from ODP Leg 104 biogenic carbonate and terrigenous records, *Palaeogeogr. Palaeoclimatol. Palaeoecol.*, *108*(1–2), 75–94, doi:10.1016/0031-0182(94)90023-X.

Heslop, D., M. J. Dekkers, and C. G. Langereis (2002), Timing and structure of the mid-Pleistocene transition: Records from the loess deposits of northern China, *Palaeogeogr. Palaeoclimatol. Palaeoecol.*, *185*(1–2), 133–143, doi:10.1016/S0031-0182(02)00282-1.

Hodell, D. A., J. E. T. Channell, J. H. Curtis, O. E. Romero, and U. Röhl (2008), Onset of "Hudson Strait" Heinrich events in the eastern North Atlantic at the end of the middle Pleistocene transition (~640 ka)?, *Paleoceanography*, *23*, PA4218, doi:10.1029/2008PA001591.

Imbrie, J., et al. (1993), On the Structure and Origin of Major Glaciation Cycles 2, *Paleoceanography*, *8*(6), 699–735, doi:10.1029/93PA02751.

Jansen, E., U. Bleil, R. Henrich, L. Kringstad, and B. Slettemark (1988), Paleoenvironmental changes in the Norwegian Sea and the Northeast Atlantic during the last 2.8 m.y.: Deep Sea Drilling Project/Ocean Drilling Program Sites 610, 642, 643 and 644, *Paleoceanography*, *3*(5), 563–581, doi:10.1029/PA003i005p00563.

Kleiven, H. F., E. Jansen, W. B. Curry, D. A. Hodell, and K. Venz (2003), Atlantic Ocean thermohaline circulation changes on orbital to suborbital timescales during the mid-Pleistocene, *Paleoceanography*, *18*(1), 1008, doi:10.1029/2001PA000629.

Kleiven, H. F., I. R. Hall, I. N. McCave, G. Knorr, and E. Jansen (2011), Coupled deep-water flow and climate variability in the middle Pleistocene North Atlantic, *Geology*, *39*(4), 343–346, doi:10.1130/G31651.1.

Knies, J., J. Matthiessen, C. Vogt, J. S. Laberg, B. O. Hjelstuen, M. Smelror, E. Larsen, K. Andreassen, T. Eidvin, and T. O. Vorren (2009), The Plio-Pleistocene glaciation of the Barents Sea-Svalbard region: A new model based on revised chronostratigraphy, *Quat. Sci. Rev.*, *28*(9–10), 812–829, doi:10.1016/j.quascirev.2008.12.002.

Krauss, W. (1986), The North Atlantic Current, *J. Geophys. Res.*, *91*(C4), 5061–5074, doi:10.1029/JC091iC04p05061.

Kucera, M., A. Rosell-Melé, R. Schneider, C. Waelbroeck, and M. Weinelt (2005), Multiproxy approach for the reconstruction of the glacial ocean surface (MARGO), *Quat. Sci. Rev.*, *24*(7–9), 813–819, doi:10.1016/j.quascirev.2004.07.017.

Larrasoaña, J. C., A. P. Roberts, E. J. Rohling, M. Winklhofer, and R. Wehausen (2003), Three million years of monsoon variability over the northern Sahara, *Clim. Dyn.*, *21*(7), 689–698, doi:10.1007/s00382-003-0355-z.

Laskar, J., P. Robutel, F. Joutel, M. Gastineau, A. C. M. Correia, and B. Levrard (2004), A long-term numerical solution for the insolation quantities of the Earth, *Astron. Astrophys.*, *428*(1), 261–285, doi:10.1051/0004-6361:20041335.

Lisiecki, L. E., and M. E. Raymo (2005), A Pliocene-Pleistocene stack of 57 globally distributed benthic $\delta^{18}O$ records, *Paleoceanography*, *20*, PA1003, doi:10.1029/2004PA001071.

Locarnini, R. A., A. V. Mishonov, J. I. Antonov, T. P. Boyer, and H. E. Garcia (2006), *World Ocean Atlas 2005*, vol. 1, *Temperature*, *NOAA Atlas NESDIS*, vol. 61, edited by S. Levitus, 182 pp., NOAA, Silver Spring, Md.

Malmgren, B. A., M. Kucera, J. Nyberg, and C. Waelbroeck (2001), Comparison of statistical and artificial neural network techniques for estimating past sea surface temperatures from planktonic foraminifer census data, *Paleoceanography*, *16*(5), 520–530, doi:10.1029/2000PA000562.

Marshall, S. J., and M. R. Koutnik (2006), Ice sheet action versus reaction: Distinguishing between Heinrich events and Dansgaard-Oeschger cycles in the North Atlantic, *Paleoceanography*, *21*, PA2021, doi:10.1029/2005PA001247.

Maslin, M. A., and A. J. Ridgwell (2005), Mid-Pleistocene revolution and the 'eccentricity myth', *Spec. Publ. Geol. Soc. Lond.*, *247*(1), 19–34, doi:10.1144/GSL.SP.2005.247.01.02.

McClymont, E. L., A. Rosell-Melé, G. H. Haug, and J. M. Lloyd (2008), Expansion of subarctic water masses in the North Atlantic and Pacific oceans and implications for mid-Pleistocene ice sheet growth, *Paleoceanography*, *23*, PA4214, doi:10.1029/2008PA001622.

McCorkle, D. C., L. D. Keigwin, B. H. Corliss, and S. R. Emerson (1990), The influence of microhabitats on the carbon isotopic composition of deep-sea benthic foraminifera, *Paleoceanography*, *5*(2), 161–185, doi:10.1029/PA005i002p00161.

McIntyre, A., and B. Molfino (1996), Forcing of Atlantic equatorial and subpolar millennial cycles by precession, *Science*, *274*(5294), 1867–1870, doi:10.1126/science.274.5294.1867.

McIntyre, A., W. F. Ruddiman, K. Karlin, and A. C. Mix (1989), Surface water response of the equatorial Atlantic Ocean to orbital forcing, *Paleoceanography*, *4*(1), 19–55, doi:10.1029/PA004i001p00019.

McIntyre, K., M. L. Delaney, and A. C. Ravelo (2001), Millennial-scale climate change and oceanic processes in the Late Pliocene and Early Pleistocene, *Paleoceanography*, *16*(5), 535–543, doi:10.1029/2000PA000526.

McManus, J. F., D. W. Oppo, and J. L. Cullen (1999), A 0.5-million-year record of millennial-scale climate variability in the North Atlantic, *Science*, *283*(5404), 971–975, doi:10.1126/science.283.5404.971.

Molfino, B., and A. McIntyre (1990), Precessional forcing of nutricline dynamics in the equatorial Atlantic, *Science*, *249*(4970), 766–769, doi:10.1126/science.249.4970.766.

Mudelsee, M., and M. Schulz (1997), The Mid-Pleistocene climate transition: Onset of 100 ka cycle lags ice volume build-up by 280 ka, *Earth Planet. Sci. Lett.*, *151*(1–2), 117–123, doi:10.1016/S0012-821X(97)00114-3.

Mudelsee, M., and K. Stattegger (1997), Exploring the structure of the mid-Pleistocene revolution with advanced methods of time-series analysis, *Geol. Rundsch.*, *86*(2), 499–511, doi:10.1007/s005310050157.

Muttoni, G., C. Carcano, E. Garzanti, M. Ghielmi, A. Piccin, R. Pini, S. Rogledi, and D. Sciunnach (2003), Onset of major Pleistocene glaciations in the Alps, *Geology*, *31*(11), 989–992, doi:10.1130/G19445.1.

Niemitz, M. D., and K. Billups (2005), Millennial-scale variability in western tropical Atlantic surface ocean hydrography during the early Pliocene, *Mar. Micropaleontol.*, *54*(3–4), 155–166, doi:10.1016/j.marmicro.2004.10.001.

Oppo, D. W., J. F. McManus, and J. L. Cullen (1998), Abrupt climate events 500,000 to 340,000 years ago: Evidence from subpolar North Atlantic sediments, *Science*, *279*(5355), 1335–1338, doi:10.1126/science.279.5355.1335.

Ortiz, J., A. Mix, S. Harris, and S. O'Connell (1999), Diffuse spectral reflectance as a proxy for percent carbonate content in North Atlantic sediments, *Paleoceanography*, *14*(2), 171–186, doi:10.1029/1998PA900021.

Paillard, D. L., and P. Yiou (1996), Macintosh program performs time-series analysis, *Eos Trans. AGU*, *77*, 379, doi:10.1029/96EO00259.

Pisias, N. G., and T. C. Moore Jr. (1981), The evolution of Pleistocene climate: A time series approach, *Earth Planet. Sci. Lett.*, *52*(2), 450–458, doi:10.1016/0012-821X(81)90197-7.

Prell, W. L. (1982), Oxygen and carbon isotope stratigraphy for the Quaternary of Hole 502B: Evidence for two modes of isotopic variability, *Initial Rep. Deep Sea Drill. Proj.*, *68*, 455–464, doi:10.2973/dsdp.proc.68.120.1982

Prell, W. L. (1985), Stability of low-latitude sea-surface temperatures: An evaluation of the CLIMAP reconstruction with emphasis on the positive SST anomalies, *Tech. Rep. DOE/ER/60167-1*, 53 pp., Dep. of Energy, Washington D. C.

Raymo, M. E., D. W. Oppo, and W. Curry (1997), The Mid-Pleistocene Climate Transition: A deep sea carbon isotopic perspective, *Paleoceanography*, *12*(4), 546–559, doi:10.1029/97PA01019.

Raymo, M. E., K. Ganley, S. Carter, D. W. Oppo, and J. McManus (1998), Millennial-scale climate instability during the early Pleistocene epoch, *Nature*, *392*(6677), 699–702, doi:10.1038/33658.

Raymo, M. E., D. W. Oppo, B. P. Flower, D. A. Hodell, J. F. McManus, K. A. Venz, K. F. Kleiven, and K. McIntyre (2004), Stability of North Atlantic water masses in face of pronounced climate variability during the Pleistocene, *Paleoceanography*, *19*, PA2008, doi:10.1029/2003PA000921.

Ruddiman, W. F. (1977), Late Quaternary deposition of ice-rafted sand in the subpolar North Atlantic (lat 40° to 65°N), *Geol. Soc. Am. Bull.*, *88*(12), 1813–1827, doi:10.1130/0016-7606(1977)88<1813:LQDOIS>2.0.CO;2.

Ruddiman, W. F., and L. K. Glover (1972), Vertical mixing of ice-rafted volcanic ash in North Atlantic sediments, *Geol. Soc. Am. Bull.*, *83*(9), 2817–2836, doi:10.1130/0016-7606(1972)83[2817:VMOIVA]2.0.CO;2.

Ruddiman, W. F., and A. McIntyre (1979), Warmth of the subpolar North Atlantic Ocean during Northern Hemisphere ice-sheet growth, *Science*, *204*(4389), 173–175, doi:10.1126/science.204.4389.173.

Ruddiman, W. F., and A. McIntyre (1981), Oceanic mechanisms for amplification of the 23,000-year ice-volume cycle, *Science*, *212*(4495), 617–627, doi:10.1126/science.212.4495.617.

Ruddiman, W. F., and A. McIntyre (1984), Ice-age thermal response and climatic role of the surface Atlantic Ocean, 40°N to 63°N, *Geol. Soc. Am. Bull.*, *95*(4), 381–396, doi:10.1130/0016-7606(1984)95<381:ITRACR>2.0.CO;2.

Sarnthein, M., U. Pflaumann, and M. Weinelt (2003), Past extent of sea ice in the northern North Atlantic inferred from foraminiferal paleotemperature estimates, *Paleoceanography*, *18*(2), 1047, doi:10.1029/2002PA000771.

Schmieder, F., T. von Dobeneck, and U. Bleil (2000), The Mid-Pleistocene climate transition as documented in the deep South Atlantic Ocean: Initiation, interim state and terminal event, *Earth Planet. Sci. Lett.*, *179*(3–4), 539–549, doi:10.1016/S0012-821X(00)00143-6.

Schmitz, W. J., Jr., and M. S. McCartney (1993), On the North Atlantic Circulation, *Rev. Geophys.*, *31*(1), 29–49, doi:10.1029/92RG02583.

Sejrup, H. P., E. Larsen, J. Landvik, E. L. King, H. Haflidason, and A. Nesje (2000), Quaternary glaciations in southern Fennoscandia: Evidence from southwestern Norway and the northern North Sea region, *Quat. Sci. Rev.*, *19*(7), 667–685, doi:10.1016/S0277-3791(99)00016-5.

Shackleton, N. J., and M. A. Hall (1984), Oxygen and carbon isotope stratigraphy of Deep Sea Drilling Project Hole 552A: Plio-Pleistocene glacial history, *Initial Rep. Deep Sea Drill. Proj.*, *81*, 599–609, doi:10.2973/dsdp.proc.81.116.1984

Shackleton, N. J., M. A. Hall, and E. Vincent (2000), Phase relationships between millennial-scale events 64,000–24,000 years ago, *Paleoceanography*, *15*(6), 565–569, doi:10.1029/2000PA000513.

Short, D. A., J. G. Mengel, T. J. Crowley, W. T. Hyde, and G. R. North (1991), Filtering of Milankovitch cycles by Earth's geography, *Quat. Res.*, *35*(2), 157–173, doi:10.1016/0033-5894(91)90064-C.

Siddall, M., E. J. Rohling, A. Almogi-Labin, C. Hemleben, D. Meischner, I. Schmelzer, and D. A. Smeed (2003), Sea-level fluctuations during the last glacial cycle, *Nature*, *423*(6942), 853–858, doi:10.1038/nature01690.

Siddall, M., T. F. Stocker, T. Blunier, R. Spahni, J. F. McManus, and E. Bard (2006), Using a maximum simplicity paleoclimate model to simulate millennial variability during the last four glacial periods, *Quat. Sci. Rev.*, *25*(23–24), 3185–3197, doi:10.1016/j.quascirev.2005.12.014.

Sierro, F. J., et al. (2009), Phase relationship between sea level and abrupt climate change, *Quat. Sci. Rev.*, *28*(25–26), 2867–2881, doi:10.1016/j.quascirev.2009.07.019.

Skinner, L. C., N. J. Shackleton, and H. Elderfield (2003), Millennial-scale variability of deep-water temperature and $\delta^{18}O_{dw}$ indicating deep-water source variations in the Northeast Atlantic, 0–34 cal. ka BP, *Geochem. Geophys. Geosyst.*, *4*(12), 1098, doi:10.1029/2003GC000585.

Steenbrink, J., M. L. Kloosterboer-van Hoeve, and F. J. Hilgen (2003), Millennial-scale climate variations recorded in Early Pliocene colour reflectance time series from the lacustrine Ptolemais Basin (NW Greece), *Global Planet. Change*, *36*(1–2), 47–75, doi:10.1016/S0921-8181(02)00163-7.

Swift, J. H., and K. Aagaard (1981), Seasonal transitions and water mass formation in the Iceland and Greenland seas, *Deep Sea Res., Part A*, *28*(10), 1107–1129, doi:10.1016/0198-0149(81)90050-9.

Vidal, L., L. Labeyrie, and T. C. E. van Weering (1998), Benthic $\delta^{18}O$ records in the North Atlantic over the last glacial period (60–10 kyr): Evidence for brine formation, *Paleoceanography*, *13*(3), 245–251, doi:10.1029/98PA00315.

Wara, M. W., A. C. Ravelo, and J. S. Revenaugh (2000), The pacemaker always rings twice, *Paleoceanography*, *15*(6), 616–624, doi:10.1029/2000PA000500.

Weirauch, D., K. Billups, and P. Martin (2008), Evolution of millennial-scale climate variability during the mid-Pleistocene, *Paleoceanography*, *23*, PA3216, doi:10.1029/2007PA001584.

Willis, K. J., A. Kleczkowski, K. M. Briggs, and C. A. Gilligan (1999), The role of sub-Milankovitch climatic forcing in the initiation of the Northern Hemisphere glaciation, *Science*, *285*(5427), 568–571, doi:10.1126/science.285.5427.568.

Wright, A. K., and B. P. Flower (2002), Surface and deep ocean circulation in the subpolar North Atlantic during the mid-Pleistocene revolution, *Paleoceanography*, *17*(4), 1068, doi:10.1029/2002PA000782.

Yiou, P., M. Ghil, J. Jouzel, D. Paillard, and R. Vautard (1994), Nonlinear variability of the climatic system from singular and power spectra of Late Quaternary records, *Clim. Dyn.*, *9*(8), 371–389, doi:10.1007/BF00207933.